Turning ZnO into an Efficient Energy Upconversion Material by Defect Engineering

*Jan E. Stehr, Shula L. Chen, Nandanapalli Koteeswara Reddy, Charles W. Tu, Weimin M. Chen, and Irina A. Buyanova**

Photon upconversion materials are attractive for a wide range of applications from medicine, biology, to photonics. Among them, ZnO is of particular interest owing to its outstanding combination of materials and physical properties. Though energy upconversion has been demonstrated in ZnO, the exact physical mechanism is still unknown, preventing control of the processes. Here, defects formed in bulk and nanostructured ZnO synthesized using standard growth techniques play a key role in promoting efficient energy upconversion via two-step two-photon absorption (TS-TPA). From photoluminescence excitation of the anti-Stokes emissions, the threshold energy of the TS-TPA process is determined as being 2.10–2.14 eV in all studied ZnO materials irrespective of the employed growth techniques. This photo-electron paramagnetic resonance studies show that this threshold closely matches the ionization energy of the zinc vacancy (a common grown-in intrinsic defect in ZnO), thereby identifying the zinc vacancy as being the dominant defect responsible for the observed efficient energy upconversion. The upconversion is found to persist even at a low excitation density, making it attractive for photonic and photovoltaic applications.

1. Introduction

ZnO is a II-VI semiconductor that holds a great promise for a variety of photonic applications owing to its wide and direct bandgap and a large exciton binding energy, combined with established growth processes that allow fabrication of ZnO with superior quality in a variety of morphologies ranging from bulk to nanostructures.[1,2] As a result, ZnO is currently considered among the key materials for UV light emitting devices, solid-state white lighting, transparent conductive oxides and UV photovoltaic cells with tailored dimensions.[3] Furthermore, as a biocompatible material, ZnO is attractive for biophotonics and bio-medical applications including cell and tissue imaging.[4]

Recently it was reported [5–7] that ZnO can also exhibit efficient photon upconversion, that is, capable of converting two low-energy photons into a single higher-energy photon, which could open a window of opportunities for improved and even new device applications. Indeed energy upconversion currently attracts great attention in diverse research fields ranging from medicine and biology to optoelectronics and photonics.[5,8–15] In biological labeling and imaging, upconversion of photoluminescence (PL) allows improved sensitivity, an increased penetration depth and spatially resolved imaging of biological objects.[9] In light emitting devices, it can be used for white light generation[10] and can also provide a new way for laser pumping,[5,11] representing a viable alternative to frequency-doubled coherent light sources. For example, by using ZnO it allows one to replace expensive UV pumping sources by existing, inexpensive visible/near-infrared laser diodes based on III-V semiconductors. This will be found advantageous for low-cost implementation of ZnO nanolasers in photonic circuits.[5] In photovoltaic devices, energy upconversion allows to increase efficiency of sunlight harvesting beyond the Shockley–Queisser limit by consumption of photons with energies below the bandgap of a light absorber.[12] Two-photon absorption was also suggested to be a potential method for information processing in three-dimensional optical storage memory[13] and has been considered as a key process in volumetric display technology.[14] We should also note that whereas energy upconversion is desirable for many applications, it may also become an obstacle when using ZnO as a transparent conductor as this process will decrease the transparency of the material for visible light.

Light upconversion in ZnO can proceed via several processes including two-photon absorption (TPA) and two-step two-photon absorption (TS-TPA).[5–7] In both processes excitation of carriers is accomplished by sequential absorption of two photons via an intermediate state. TPA occurs via a virtual state and thus requires rather high excitation densities (i.e., of the order of $P_{exc} = 10^9$ W cm^{-2}) in spite of a lack of inversion symmetry adherent to the wurtzite crystal structure of

Dr. J. E. Stehr, S. L. Chen, Prof. W. M. Chen, Prof. I. A. Buyanova
Department of Physics Chemistry and Biology
Linköping University
581 83, Linköping, Sweden
E-mail: iribu@ifm.liu.se
Dr. N. K. Reddy
Department of Nanobio Materials and Electronics
Gwangju Institute of Science and Technology
Gwangju 500712, Republic of Korea
Prof. C. W. Tu
Department of Electrical and Computer Engineering
University of California
La Jolla, CA 92093, USA

DOI: 10.1002/adfm.201400220

this material. On the other hand, TS-TPA can be achieved at remarkably low $P_{exc} \approx 0.1$ W cm^{-2}[7] owing to the fact that the intermediate state involved in this process is a real state, for example, an energy level of a defect or impurity. This process therefore dominates in low excitation density regimes and has the benefit of relatively high (i.e., in the order of 1–2% at low P_{exc}) conversion efficiency without the need for intense excitation sources.

Optimization of the TS-TPA process requires in-depth understanding of material properties so that defects/impurities which introduce the intermediate state are first reliably identified and then deliberately incorporated in (or removed from) the material. Such understanding, however, is currently lacking. The key questions, that is, what is the origin of the defect/impurity responsible for the TS-TPA process in ZnO and the exact energy position of the corresponding intermediate state, remain unanswered, though we have most recently suggested[7] that a native defect may be involved. The purpose of the present work is to reliably answer these questions based on comprehensive electron paramagnetic resonance (EPR) studies combined with detailed spectral dependent measurements of TS-TPA. The EPR spectroscopy is chosen in this study as this technique, together with its optical counterpart—optically detected magnetic resonance (ODMR)—is among the most powerful and versatile experimental methods for defect identification. It has been used in the past to provide chemical identity and local structure of various intrinsic defects and impurities in ZnO, and also to determine their energy level positions within the bandgap.[16,17] Furthermore, knowledge gained from spectral dependence of TS-TPA based on excitation spectroscopy of upconverted PL will allow us to accurately determine the energy position of the intermediate level involved in the upconversion, which could then be correlated with the results of EPR studies to uncover the defect identity.

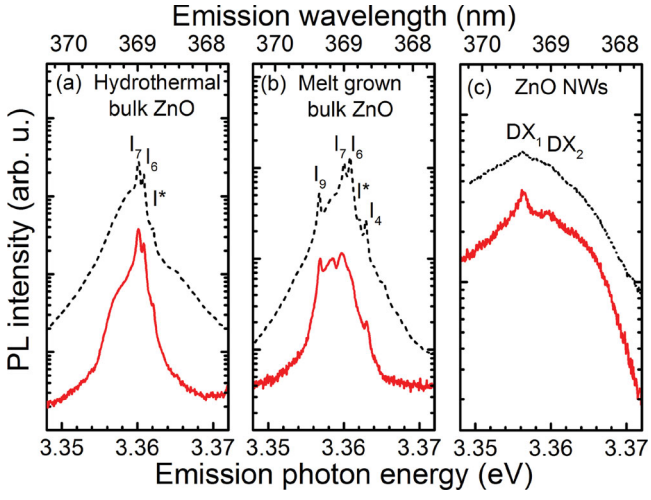

Figure 1. Representative PL spectra measured within the excitonic spectral range from a) bulk hydrothermal and b) melt-grown ZnO and also from c) ZnO NWs. The solid (red online) and dashed (black online) lines represent spectra measured under two-photon (λ_{exc} = 400 nm) and one-photon (λ_{exc} = 266 nm) excitation, respectively. The spectra are displayed in the semi-logarithmic scale and are offset vertically, for clarity.

2. Results and Discussion

In order to evaluate whether the TS-TPA process in ZnO has a common origin, several types of ZnO synthesized using standard growth techniques were selected for this study. These include commercially available melt-grown and hydrothermally-grown bulk substrates and ZnO nanowires (NWs) grown by rapid thermal chemical vapor deposition on c-plane Al_2O_3 substrates. Light upconversion was monitored by the intensity of donor bound exciton (BX) emissions.

All investigated structures exhibit energy upconversion, obvious from the appearance of intense near-band-edge emissions due to BX recombination under anti-Stokes excitation by visible light. This is demonstrated in **Figure 1**, which shows representative PL spectra measured with λ_{exc} = 400 nm (the solid lines). The spectra of the bulk materials (Figure 1a,b) contain well-known BX lines labeled as I_9, I_7, I_6, I_4, and I* adopting the notations from Reference.[18,19] Some of these lines (e.g., I_9, and I_7) are also likely detected in the ZnO NWs, though broadened and shifted by about 0.5 meV relative to their energy positions in bulk ZnO. These lines are labeled in Figure 1c as DX_1 and DX_2, respectively. All these spectra are very similar to those measured under conventional one-photon excitation with λ_{exc} = 266 nm above the ZnO bandgap energy (shown by the dashed lines in Figure 1). The relative contributions of different excitonic emissions vary between the one- and two-photon excitation conditions, however, likely due to strong re-absorption effects that become important in the latter case.

The observed energy upconversion can be accomplished within a wide spectral range of 380 – 735 nm, due to combined effects of TPA and TS-TPA. Contributions of these processes can be differentiated by measuring dependence of the upconverted PL (UPL) intensity, $I_{UPL,}$ on P_{exc}. Indeed, in the case of TPA, the UPL intensity increases quadratically with P_{exc}, that is, $I_{UPL} \approx P n_{exc}$ with $n = 2$, whereas a weaker power dependence with n < 2 is typical for TS-TPA via a long-lived real state. Our detailed power-dependent measurements of the studied structures using light sources with a fixed wavelength [7] have shown that TPA can be detected for all photons with wavelengths between 380 and 735 nm but prevails at high $P_{exc} > 10$ W cm^{-2}. It is also the only process responsible for the UPL excitation for λ_{exc} = 661–735 nm. On the other hand, TS-TPA allows efficient energy upconversion in the very weak excitation regime (i.e., for P_{exc} as low as 0.1–10 W cm^{-2}) and has a spectral threshold somewhere between 532 and 661 nm.

To determine the exact energy position of the involved intermediate state, we have performed PLE measurements using a tunable dye-laser. **Figure 2** shows the dependence of the BX UPL intensity divided by P^2_{exc} measured from the a) bulk and b) NW ZnO. Presenting data in these coordinates allows us to precisely determine the spectral threshold of the TS-TPA process, as the I_{UPL}/P^2_{exc} ratio is expected to remain constant when the TPA process dominates. The latter is indeed the case when λ_{exc} exceeds 590 nm, which proves that the energy upconversion under these conditions occurs solely via TPA. On the other hand, a steep rise of the UPL efficiency is observed when λ_{exc} is tuned shorter than 590 nm. This suggests activation of an additional upconversion process via TS-TPA as shown schematically in Figure 2c. This assignment was further confirmed

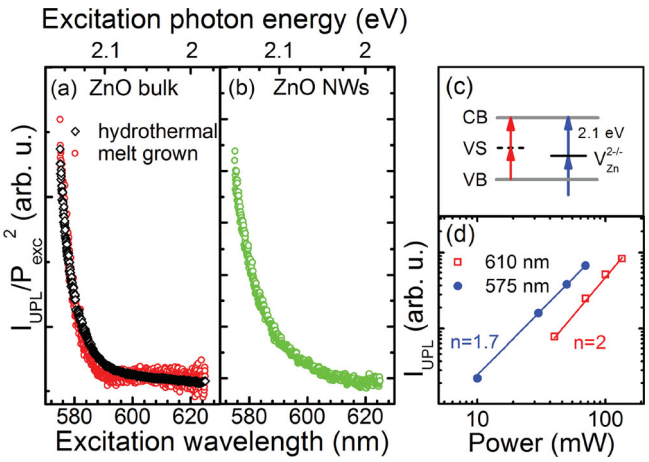

Figure 2. PLE spectra measured at 5 K by monitoring the dominant UPL emission from the a) bulk and b) NWs samples. c) Schematic picture of the TPA and TS-TPA processes via virtual and real defect (zinc vacancy) states, which are labeled as VS and V_{Zn}, respectively. d) Excitation power dependences of the UPL emission measured from the bulk ZnO with λ_{exc} = 575 nm (the solid dots) and 610 nm (open squares). The data are displayed in a double-logarithmic scale. The solid lines represent fits by the relation $I_{UPL} \approx P^n_{exc}$ with the specified n.

from excitation power dependent measurements performed for several λ_{exc} in the vicinity of the threshold. Taking as an example the bulk ZnO, the corresponding results for λ_{exc} = 575 and 610 nm are shown in Figure 2d by the filled circles and open squares, respectively. A best fit to the experimental data using the power-law function yields n = 1.7 and 2 for λ_{exc} = 575 and 610 nm, respectively. The observed decrease in the power-law factor n for λ_{exc} < 590 nm further proves that the energy upconversion now involves TS-TPA. It also implies that the energy level of the defect/impurity responsible for the two-photon absorption is located at 2.10–2.14 eV below the conduction band or above the valence band. As also seen from Figure 2 this threshold energy is the same for all studied ZnO materials irrespective of the employed growth methods. This finding suggests that the TS-TPA process in ZnO is promoted by the same defect/impurity that is commonly present in ZnO.

In order to identify the chemical origin of the responsible defect/impurity, we performed photo-EPR experiments. This is because a unique set of spin-Hamiltonian parameters determined from photo-EPR for each defect/impurity can be used as a fingerprint of the particular defect/impurity. Furthermore, an EPR signal can only be detected when the studied center is in a paramagnetic charge state with an unpaired electron spin. In dark, the charge state of the center is determined by the Fermi level position in the sample. The charge state can, however, be changed upon light illumination, provided that the photon energy is sufficient for photo-ionization of the involved defect/impurity. This makes possible to use photo-EPR measurements to determine energy level positions of various defects present in the samples and then to correlate them with the spectral threshold for the TS-TPA process. EPR results were analysed with the help of Easyspin[20] using the following spin Hamiltonian:

$$\mathbf{H} = \mu_B \mathbf{BgS} + \mathbf{SDS} + \mathbf{SAI} \quad (1)$$

Here, the first term denotes the electronic Zeeman energy, with the Bohr magneton μ_B, the external magnetic field **B**, the electron spin **S**, and the electron g-tensor **g**. The fine structure splitting for $S > ½$ is given by the second term with its interaction tensor **D**. The third term describes the hyperfine interaction involving the nuclear spin I, quantified by the hyperfine tensor **A**. The terms representing nuclear quadrupole and nuclear Zeeman interactions are omitted from Equation 1 as they play a negligible role in EPR spectra, except that the former may partially relax the selection rule of EPR transitions by admixing of nuclear spin states when $I > ½$. The spin-Hamiltonian parameters of all detected EPR signals are summarized in **Table 1**. These include common contaminants, such as Mn, Fe, Li, Al, and Ga impurities, as well as intrinsic defects such as oxygen (V_O) and zinc (V_{Zn}) vacancies.

Contributions of the aforementioned EPR signals were found to be material-dependent and were also affected by experimental conditions, that is, light illumination and photon wavelength. To demonstrate these effects, **Figure 3**a shows representative EPR spectra measured at 77 K in dark and under light illumination, taking as an example the melt-grown bulk ZnO. In dark, the EPR spectrum contains two signals. The first one, which is centered at 343.5 mT with a line width of approximately 1 mT, is denoted by EM and originates from a

Table 1. Summary of the spin-Hamiltonian parameters of the defects discussed in this work. The axial components of the electron **g**-tensor are denoted as $g_\perp$ and $g_\parallel$, while the components for the non-axial centers are given by g_{xx}, g_{yy}, and g_{zz}. For the non-axial centers, φ is the angle between the ***z*** and ***c*** axis. The perpendicular and parallel components $A_\perp$ and $A_\parallel$ of the hyperfine interaction tensor **A** and the fine structure parameter D are given in MHz. With $D_{zz} = 2D/3$ and $D_{xx} = D_{yy} = -D/3$. The parallel and perpendicular directions are with respect to the ***c***-axis.

Center	S	I	g_{xx} ($g_\perp$) g_{yy}	g_{zz} ($g_\parallel$)	$\lvert A_\perp \rvert$	$\lvert A_\parallel \rvert$	D	φ [deg]
V_{Zn}^- (axial)	1/2		2.0193	2.0041				
V_{Zn}^- (non-axial)	1/2		2.0173 2.0183	2.0041				110.75
Li^0 (axial)	1/2	3/2	2.0253	2.0028	5.12	0.61		
Li^0 (non-axial)	1/2	3/2	2.0223 2.0254	2.0040	5.1	0.81		3.1
V_O^+	1/2		1.9960	1.9945				
EM	1/2		1.955	1.957				
Fe^{3+}	5/2	1/2	2.0060	2.0060	27.04	27.04	–1779.9	
Mn^{2+}	5/2	5/2	2.0016	2.0016	227.8	227.8	–650.2	

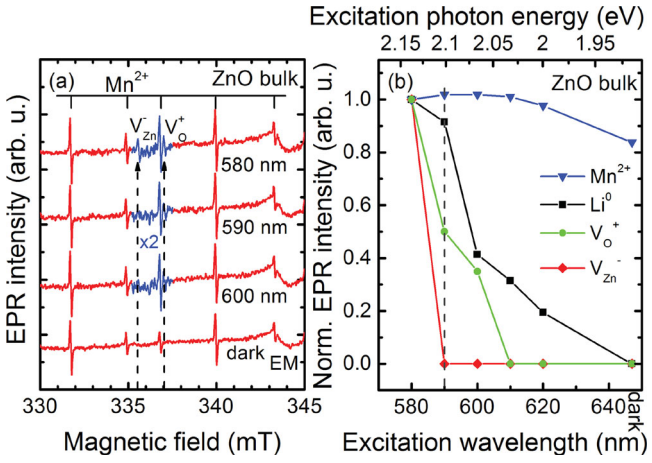

Figure 3. a) EPR spectra from the melt-grown ZnO measured at 77 K with a microwave frequency of 9.4 GHz in dark and under light illumination. An applied magnetic field was oriented parallel to the c-axis of the ZnO crystal. b) Intensities of the detected EPR signals as a function of excitation wavelength. All data are normalized to the same peak intensity. The dashed line represents the spectral threshold for the TS-TPA process deduced from the PLE measurements of the UPL emission.

shallow effective mass donor, likely an Al and/or a Ga impurity. The second signal spans over a wide range of magnetic fields (210–460 mT) and consists of five groups of six lines, which clearly indicates involvement of a paramagnetic center with $S = 5/2$ and $I = 5/2$. This signal is an EPR signature of a Mn^{2+} ion.[21] Illumination at the wavelength of 610 nm does not change the EPR spectra. However, when the light wavelength is decreased to 600 nm an EPR signal from the positively changed V_O^+ center[22] is activated as a result of the light-induced photo-ionization which converts V_O from the neutral to positively charged state:

$$V_O^0 + h\upsilon \rightarrow V_O^+ + e \quad (2)$$

This places the (0/+) level of this defect at around 2.0 eV below the conduction band, consistent with previous photo-EPR studies.[22] At an even shorter wavelength of 580 nm, another EPR signal appears at 335.6 mT. Based on the determined spin-Hamiltonian parameters, this signal can be attributed to the negatively charged axial V_{Zn}^-.[24] The corresponding photo-ionization process,

$$V_{Zn}^{2-} + h\upsilon \rightarrow V_{Zn}^- + e \quad (3)$$

has a threshold at around 2.1 eV in agreement with previously reported data.[1,23,24] In addition to Mn^{2+}, V_O^+, and V_{Zn}^- that dominate in the melt-grown ZnO discussed above, hydrothermally grown materials were found to contain Fe and Li that give rise to EPR signals arising from a neutral Li acceptor, Li_{Zn}^0,[25] and a positive Fe^{3+} ion located at a Zn site. The Li_{Zn}^0 was only observed under illumination with $\lambda_{exc} < 650$ nm, whereas the Fe^{3+} signal could also be detected in dark. Other common trace impurities, such as Ni, Cu, and Pb that are known to introduce deep levels in the bandgap of ZnO,[16,26] were not present in sufficient concentrations to be detected by photo-EPR and thus to contribute to the observed TS-TPA.

The illumination wavelength dependences of the EPR signals measured from the investigated bulk ZnO samples are summarized in Figure 3b. It is obvious that though several defects and impurities participate in the light absorption within the visible spectral range, only V_{Zn} has the energy level that exactly matches the spectral threshold of the TS-TPA deduced from the PLE measurements shown in Figure 3b. This provides compelling evidence that the zinc vacancy is the dominant defect responsible for the observed TS-TPA process in bulk ZnO. Moreover, an increase in the upconversion efficiency was observed for materials with a higher V_{Zn} concentration, which further supports this conclusion.

From the PLE measurements (Figure 2), the same defects are also expected to be responsible for the TS-TPA in ZnO NWs. Unfortunately, the total number of the zinc vacancies was found to be below the EPR detection limit, because of a small NW volume. In order to confirm formation of the V_{Zn} defects in the studied NWs, we have resorted to the ODMR technique that has a significantly higher sensitivity due to optical detection.[27] Strong ODMR signals from the axial and non-axial V_{Zn}^- centers were indeed detected[7,28] when monitoring visible light emissions, providing an unambiguous experimental proof for the formation of the zinc vacancies in the studied ZnO NWs. Together with the observed threshold of the TS-TPA upconversion process that coincides with the onset of the photon-ionization of the V_{Zn}^{2-}, that is, the (2–/–) level of V_{Zn}, this allows us to conclude that the V_{Zn} defects also plays a dominant role in the energy upconversion in the ZnO NWs.

3. Conclusion

In summary, we have demonstrated that defects commonly present in bulk and nanostructured ZnO can in fact extend functionality of this material as they can mediate efficient energy upconversion via the TS-TPA process. We have accurately determined the energy threshold of the process as being 2.10–2.14 eV. This threshold is found to be practically identical for all investigated materials irrespective of the employed growth techniques, which suggests that the intermediate state involved in the energy upconversion belongs to the same defect. Using photo-EPR we show that among all common contaminants and intrinsic defects, only the zinc vacancy has the ionization energy that closely matches the TS-TPA onset. The presence of this defect is also revealed in all materials that exhibit the TS-TPA. The obtained results thus provide compelling evidence that the zinc vacancy is the dominant defect responsible for the observed energy upconversion in bulk and nanostructured ZnO. This work shows that the defect-mediated TS-TPA process can turn ZnO into an efficient energy-upconversion material without resorting to high photon densities, which can be exploited for a variety of applications in optoelectronics and photovoltaics. By identifying the chemical nature and the energy level of the defect responsible for TS-TPA, our finding also provides a useful guideline for further defect engineering of the energy upconversion efficiency by purposely incorporating the zinc vacancy defect, or by removing it if the associated energy upconversion process will be found detrimental to device applications for transparent electronics.

4. Experimental Section

All structures investigated in this work were intentionally undoped. Bulk melt-grown ZnO single crystals from Cermet Inc. were n-type conductive with a carrier concentration ranging between 1×10^{16} and 2×10^{17} cm^{-3}. The electron concentration was lower in hydrothermally-grown ZnO from Tokyo Denpa Co, that is, around 5–9 $\times 10^{15}$ cm^{-3}. The ZnO NWs were grown on Au coated sapphire substrates using rapid thermal chemical vapor deposition (RTCVD) at 950 °C. The growth was performed at a pressure of 20 Torr under the Ar and O_2 flow as described in detail in the literature.[29] All samples have superior optical quality evident from the predominance of the BX emissions and only a weak (about 5–10%) contribution of defect-related emissions in PL spectra within the visible spectral range.

The anti-stokes (or upconverted) PL was excited by using either second-harmonic pulses (λ_{exc} = 350–450 nm) of a tunable mode-locked Ti:sapphire solid state laser, with a pulse duration of 2 ps and a repetition rate of 76 MHz, or a dye laser tunable within the 575–700 nm spectral range. The 266 nm line from a solid-state laser was used for the one-photon excitation above the bandgap energy. The incident laser beam was focused to a spot diameter of ≈ 0.5 mm. The PL signals were detected at 5 K either by a photomultiplier tube assembled with a 0.8 m double-grating monochromator or by a streak camera combined with a 0.5 m single-grating monochromator. EPR measurements were carried out at temperatures between 4.2 and 77 K with a microwave frequency of ≈ 9 GHz. For photo-EPR investigations the same tunable dye laser as the one employed in the PL experiments was used. Before each photo-EPR measurement, the sample was cooled down in dark from room temperature to 77 K prior to 3 min light illumination with a given photon energy. This was done to ensure the same initial condition for each measurement and also to avoid effects of ambient light and photo-induced recharging from preceding measurements. ODMR studies were performed at 3K with a microwave (MW) frequency of ≈ 9 GHz using the 364 nm line of an Ar^+ ion laser as an excitation source. ODMR spectra were obtained as a change of the integrated PL intensity detected by a Si detector within the visible spectral range of 420–1000 nm.

Acknowledgements

The financial support of this work by the Swedish Research Council (grant # 621–2010–3971) is greatly appreciated.

Received: January 21, 2014
Published online: March 31, 2014

[1] A. Janotti, C. G. Van de Walle, *Rep. Prog. Phys.* **2009**, *72*, 126501.
[2] a) S. J. Pearton, D. P. Norton, M. P. Ivill, A. F. Hebard, J. M. Zavada, W. M. Chen, I. A. Buyanova, *IEEE Trans. Electron Dev.* **2007**, *54*, 1040; b) C. M. Lieber, Z. L. Wang, *MRS Bull.* **2007**, *22*, 99.
[3] a) M. H. Huang, S. Mao, H. Feick, H. Yan, Y. Wu, H. Kind, E. Weber, R. Russo, P. Yang, *Science* **2001**, *292*, 1897; b) M. Law, L. E. Greene, J. C. Johnson, R. Saykally, P. Yang, *Nat. Mater.* **2005**, *4*, 455; c) J. J. Cole, X. Wang, R. J. Knuesel, H. O. Jacobs, *Nano Lett.* **2008**, *8*, 1477.
[4] a) Y. L. Wu, C. S. Lim, S. Fu, A. I. Y. Tok, H. M. Lau, F. Y. C. Boey, X. T. Zeng, *Nanotechnology* **2007**, *18*, 215604; b) H.-M. Xiong, *Adv. Mater.* **2013**, *25*, 5329.
[5] C. Zhang, F. Zhang, T. Xia, N. Kumar, J. Hahm, J. Liu, Z. L. Wang, J. Xu, *Opt. Express* **2009**, *17*, 7893.
[6] a) Y. C. Zhong, K. S. Wong, A. B. Djurišic, Y. F. Hsu, *Appl. Phys. B* **2009**, *97*, 125; b) C. F. Zhang, Z. W. Dong, G. J. You, R. Y. Zhu, S. X. Qian, H. Deng, H. Cheng, J. C. Wang, *Appl. Phys. Lett.* **2006**, *89*, 042117; c) W. Cao, W. Du, F. Su, G. Li, *Appl. Phys. Lett.* **2006**, *89*, 031902; d) S. Mani, J. I. Jang, J. B. Ketterson, *Appl. Phys. Lett.* **2008**, *93*, 041902; e) S. K. Das, M. Biswas, D. Byrne, M. Bock, E. McGlynn, M. Breusing, R. Grunwald, *J. Appl. Phys.* **2010**, *108*, 043107.
[7] S. L. Chen, J. Stehr, N. K. Reddy, C. W. Tu, W. M. Chen, I. A. Buyanova, *Appl. Phys. B* **2012**, *108*, 919.
[8] F. Auzel, *Chem. Rev.* **2004**, *104*, 139.
[9] a) F. van de Rijke, H. Zijlmans, S. Li, T. Vail, A. K. Raap, R. S. Niedbala, H. J. Tanke, *Nat. Biothechnol.* **2001**, *19*, 273; b) S. F. Lim, R. Riehn, W. S. Ryu, N. Khanarian, C. K. Tung, D. Tank, R. H. Austin, *Nano Lett.* **2006**, *6*, 169; c) M. Nyk, R. Kumar, T. Y. Ohulchanskyy, E. J. Bergey, P. N. Prasad, *Nano Lett.* **2008**, *8*, 3834; d) B. E. Cohen, *Nature* **2010**, *467*, 407; e) F. Wang, Y. Han, C. S. Lim, Y. Lu, J. Wang, J. Xu, H. Chen, C. Zhang, M. Hong, X. Liu, *Nature* **2010**, *463*, 1061.
[10] S. Sivakumar, F. C. J. M. van Veggel, M. J. Raudsepp, *J. Am. Chem. Soc.* **2005**, *127*, 12464.
[11] S. L. Oliveira, D. S. Corrêa, L. Misoguti, C. J. L. Constantino, R. F. Aroca, S. C. Zilio, C. R. Mendonça, *Adv. Mater.* **2005**, *17*, 1890.
[12] a) B. M. van der Ende, L. Aarts, A. Meijerink, *Phys. Chem. Chem. Phys.* **2009**, *11*, 11081; b) G.-B. Shan, G. P. Demopoulos, *Adv. Mater.* **2010**, *22*, 4373; c) W. Zou, C. Visser, J. A. Maduro, M. S. Pshenichnikov, J. C. Hummelen, *Nat. Photonics* **2012**, *6*, 560.
[13] D. A. Parthenopoulos, P. M. Rentzepis, *Science* **1989**, *245*, 843.
[14] E. Downing, L. Hesselink, J. Ralston, R. Macfarlane, *Science* **1996**, *273*, 1185.
[15] F. Wang, R. Deng, J. Wang, Q. Wang, Y. Han, H. Zhu, X. Chen, X. Liu, *Nat. Mater.* **2011**, *10*, 968.
[16] V. A. Nikitenko, *J. Appl. Spectrosc.* **1992**, *57*, 783.
[17] J. E. Stehr, B. K. Meyer, D. M. Hofmann, *Appl. Magn. Reson.* **2010**, *39*, 137.
[18] B. K. Meyer, H. Alves, D. M. Hofmann, W. Kriegseis, D. Forster, F. Bertram, J. Christen, A. Hoffmann, M. Straßburg, M. Dworzak, U. Haboeck, A. V. Rodina, *Phys. Status Solidi B* **2004**, *241*, 231.
[19] S. L. Chen, W. M. Chen, I. A. Buyanova, *Phys. Rev. B* **2012**, *86*, 235205.
[20] S. Stoll, A. Schweiger, *J. Magn. Reson.* **2006**, *178*, 42.
[21] P. Dorain, *Phys. Rev.* **1958**, *112*, 1058.
[22] a) J. M. Smith, W. E. Vehse, *Phys. Lett. A* **1970**, *31*, 147; b) C. Gonzalez, D. Galland, A. Herve, *Phys. Status Solidi B* **1975**, *72*, 309.
[23] a) X. J. Wang, L. S. Vlasenko, S. J. Pearton, W. M. Chen, I. A. Buyanova, *J. Phys. D. Appl. Phys.* **2009**, *42*, 175411; b) S. M. Evans, N. C. Giles, L. E. Halliburton, L. A. Kappers, *J. Appl. Phys.* **2008**, *103*, 043710; c) R. Laiho, L. S. Vlasenko, M. P. Vlasenko, *J. Appl. Phys.* **2008**, *103*, 123709.
[24] D. Galland, A. Herve, *Phys. Lett. A* **1970**, *33*, 1.
[25] P. H. Kasai, *Phys. Rev* **1963**, *130*, 989.
[26] M. D. McCluskey, S. J. Jokela, *J. Appl. Phys.* **2009**, *106*, 071101.
[27] W. M. Chen, *Thin Solid Films* **2000**, *364*, 45.
[28] J. E. Stehr, S. L. Chen, S. Filippov, M. Devika, N. Koteeswara Reddy, C. W. Tu, W. M. Chen, I. A. Buyanova, *Nanotechnology* **2013**, *24*, 015701.
[29] Q. J. Ren, S. Filippov, S. L. Chen, M. Devika, N. Koteeswara Reddy, C. W. Tu, W. M. Chen, I. A. Buyanova, *Nanotechnology* **2012**, *23*, 425201.